Fast LISA response functions for massive black hole binaries

Author: Mireia Egido Quesada, megidoqu7@alumnes.ub.edu
Facultat de Física, Universitat de Barcelona, Diagonal 645, 08028 Barcelona, Spain.

Advisor: Carlos F. Sopuerta, carlos.f.sopuerta@csic.es and
Tutor: Ruxandra Bondarescu, ruxandra.bondarescu@ub.edu

Abstract: LISA is a space-based gravitational wave observatory under development by the European Space Agency (ESA), designed to detect low-frequency signals from sources such as massive and stellar-mass black hole binaries. To process the signals LISA (Laser Interferometer Space Antenna) will observe, it is necessary to model its detector response accurately. In this work, we implement LISA's noise-free frequency-domain response using the IMRPhenomD waveform model. The response is implemented in JAX, which provides efficient numerical computation and support for automatic differentiation. Our model accounts for the constellation's motion and Time Delay Interferometry (TDI) observables. We validate the resulting strain signals using the BBHx simulation code, finding overlaps above 0.99999999 across all TDI channels and mass ranges, which demonstrates the reliability of our implementation.
Keywords: Gravitational waves, Interferometry, Numerical Modeling, Fourier Analysis
SDGs: This work is relate to the Sustainable Development Goal (SDG) 9.

I. INTRODUCTION

Gravitational waves (GW) were first detected in 2015 by the LIGO detectors in the United States. Since then, a total of 90 confirmed gravitational wave events have been observed. However, as these detectors are ground-based interferometers, terrestrial noise limits our ability to detect low-frequency signals. This prevents us from studying mergers of compact objects with masses greater than a few $10^2 M_{\odot}$.

To overcome this limitation, the LISA project was proposed in the 1990s with a design that has remained essentially unchanged: three spacecrafts deployed in a single launch. With LISA, we will be able to explore a frequency range inaccessible to LIGO, allowing us to study systems such as massive black hole binaries (MBHB) and stellar-mass black hole binaries (SBHB). While the LIGO-Virgo collaboration detects GWs in the range of 50 to 2000 Hz, LISA will detect GWs with much lower frequencies, ranging from 0.0001 to 0.1 Hz.

Accurately detecting and interpreting gravitational wave signals requires modeling how theoretical waveforms translate into measurable responses at the detector. A critical step in this process is computing how a model waveform, such as those generated by the IMRPhenomD family ([4], [5]), would appear in LISA's data. This involves simulating the detector response, accounting for the constellation's motion, the effects of time delay interferometry (TDI), and the geometric projection onto the spacecraft arms. The goal of this work is to implement and analyze this response in the frequency domain, providing a framework for transforming idealized waveforms into realistic signals as LISA would observe them.

To validate the strain signal produced by our implementation, we rely on BBHx as an external reference. The response function used in this work is implemented entirely in JAX, a Python library designed for high-performance numerical computing that supports just-in-time compilation and automatic differentiation. These features make it particularly well suited for applications involving large-scale simulations and gradient-based analysis. The waveform itself is generated using a JAX version of the IMRPhenomD model, which was developed during my internship.

II. LISA RESPONSE FUNCTION

Before introducing the LISA detector model, we summarize the key assumptions of our implementation ([1]). Since our goal is to compute the frequency-domain response and evaluate its accuracy, higher-order corrections relevant for noise cancellation are omitted but could be added later.

We neglect relativistic effects of order v/c, including Doppler shifts from spacecraft motion, and treat spacetime as flat, ignoring gravitational redshift and light deflection by the Sun. Geometric quantities are evaluated simultaneously, without accounting for light travel time between spacecraft. The constellation is modeled as a rigid, equilateral triangle with fixed arm lengths, neglecting second-order eccentricity and external perturbations.

Theoretical gravitational wave models (such as IMRPhenomD) generate the signal as it would be observed by a detector located at the Solar System Barycentre (SSB). However, LISA is not stationary: it orbits the Sun, and its centre of mass follows a time-dependent trajectory $p_0(t)$. Because of this, the total response naturally splits into two parts: an orbital delay, and the constellation response.

The first component, the orbital delay, involves applying a time shift to propagate the gravitational wave from the SSB to the centre of LISA's triangular constellation. This delay is the same for all observables y_{slr}. Letting

h^{TT} represent the transverse-traceless gravitational wave tensor, the orbital delay can be expressed as

$$h_0^{TT}(t) = h^{TT}(t - k \cdot p_0/c), \tag{1}$$

where k is the unit vector in the direction of wave propagation.

The second component of the response corresponds to the projection of the gravitational wave onto the arms of the constellation. For a signal travelling from spacecraft s to r along arm l, the one-way fractional frequency shift is

$$\begin{aligned} y_{slr} &= \frac{\nu_r - \nu_s}{\nu} = \\ &= \frac{1}{2}\frac{n_l^i n_l^j}{1 - k \cdot n_l}[h_{ij}^{TT}(t - L/c - k \cdot p_s/c) - h_{ij}^{TT}(t - k \cdot p_r/c)], \end{aligned} \tag{2}$$

where n_l is the unit vector along the arm between the spacecraft, L is the armlength, and p_s, p_r are the positions of the sending and receiving spacecrafts, respectively. This expression, known as the detector response, describes how LISA measures the effect of a passing gravitational wave.

A. The LISA constellation

To describe the motion of LISA's spacecraft, we separate the heliocentric orbit of the constellation from the internal triangular configuration. The position of each spacecraft relative to the constellation centre is given to first order in the eccentricity, following Ref. [2]:

$$\begin{aligned} \vec{p}_n^L &= Re[\sin\alpha(t)\cos\alpha(t)\sin\beta_n - (1 + \sin^2\alpha(t))\cos\beta_n]\hat{x} \\ &+ Re[\sin\alpha(t)\cos\alpha(t)\cos\beta_n - (1 + \cos^2\alpha(t))\sin\beta_n]\hat{y} \\ &- \sqrt{3}Re\cos(\alpha(t) - \beta_n)\hat{z}, \end{aligned} \tag{3}$$

where $\alpha(t) = 2\pi f_m(t - t_0) + \kappa$ is the orbital phase, $\beta_n = \frac{2\pi(n-1)}{3} + \lambda$ defines each spacecraft's orientation, and $f_m = 1/\text{yr}$. The parameters λ and κ set the initial orientation of the constellation, and the eccentricity is $e = \frac{L}{2\sqrt{3}R}$, with L the arm length and R the orbital radius.

On the other hand, the position of each spacecraft in the SSB frame can be expressed as

$$\vec{p}_n = \vec{p}_n^L + \vec{p}_0\,, \qquad \vec{p}_0 = R\cos\alpha(t)\hat{x} + R\sin\alpha(t)\hat{y}, \tag{4}$$

where $\vec{p}_0$ denotes the position of the centre of the LISA constellation.

B. Fourier transform of the signal

To efficiently compute the detector response in the frequency domain, we adopt a transfer function formalism ([1], [2]), where the signal is expressed as a modulation of the waveform:

$$\widetilde{s}(f) = \mathcal{T}(f)\widetilde{h}(f). \tag{5}$$

In this framework, the frequency-domain response is characterized by a complex transfer function $\mathcal{T}(f)$ that encodes both amplitude and phase modulations induced by LISA's motion and geometry. A detailed derivation of this formalism is provided in Appendix A.

For each elementary link in the constellation, the transfer function can be approximated analytically by evaluating the kernel at a representative signal-dependent time t_f, yielding:

$$\mathcal{T}_{slr}(f) = G_{slr}(f, t_f), \tag{6}$$

where $G_{slr}(f,t)$ is given by

$$\begin{aligned} G_{slr} &= \frac{i\pi f L}{c} sinc[\pi f L/c(1 - k \cdot n_l)] \\ &\cdot \exp\{i\pi f[L + k \cdot (p_r + p_s)]/c\} n_l \cdot P_{lm} \cdot n_l, \end{aligned} \tag{7}$$

and the signal-dependent time t_f by

$$t_f = -\frac{1}{2\pi}\frac{d\Psi}{df}. \tag{8}$$

C. Time Delay Interferometry

To extract the gravitational wave signal from the raw LISA measurements, we apply Time Delay Interferometry (TDI), which constructs laser-noise-canceling observables by combining the phase measurements from different arms with appropriate time delays (see Appendix B for details).

Defining $z \equiv \exp(2i\pi f L/c)$, the reduced TDI channels can be written in terms of the y_{slr} observables as

$$\tilde{a} = (1 + z)(\tilde{y}_{31} + \tilde{y}_{13}) - \tilde{y}_{23} - z\tilde{y}_{32} - \tilde{y}_{21} - z\tilde{y}_{12} \tag{9a}$$

$$\begin{aligned} \tilde{e} = \frac{1}{\sqrt{3}}[&(1 - z)(\tilde{y}_{13} - \tilde{y}_{31}) + (2 + z)(\tilde{y}_{12} - \tilde{y}_{32}) \\ &+ (1 + 2z)(\tilde{y}_{21} - \tilde{y}_{23})] \end{aligned} \tag{9b}$$

$$\tilde{t} = \sqrt{\frac{2}{3}}[\tilde{y}_{21} - \tilde{y}_{12} + \tilde{y}_{32} - \tilde{y}_{23} + \tilde{y}_{13} - \tilde{y}_{31}]. \tag{9c}$$

Each of these channels can be modelled as the product of a transfer function and the gravitational waveform in frequency space:

$$\tilde{a}, \tilde{e}, \tilde{t} = \mathcal{T}_{a,e,t}(f)\tilde{h}(f), \tag{10}$$

and rescaled to define the strain response via:

$$\tilde{h}_{a,e,t} \equiv \frac{1}{-6i\pi f L/c} \times \tilde{a}, \tilde{e}, \tilde{t}, \tag{11a}$$

$$\mathcal{T}_{h_a,h_e,h_t}(f) \equiv \frac{1}{-6i\pi f L/c}, \mathcal{T}_{a,e,t}(f). \quad (11b)$$

These expressions provide a compact and computationally convenient way to model the detector's response to an incoming gravitational wave across all three TDI channels.

III. COMPUTATION OF THE RESPONSE FUNCTION

A. Doppler phase

To study the response in a realistic setting, we consider a representative MBHB system expected in LISA's observations. The redshifted component masses are $m_1 = 1.5 \times 10^6$ M$\odot$ and $m_2 = 0.5 \times 10^6$ M$\odot$, giving a total mass $M = 2 \times 10^6$ M$_\odot$ and a mass ratio $q = 3$, located at redshift $z = 4$. In the low-frequency regime ($f \ll f_L$), the kernel in Eq. 7 simplifies accordingly.

$$G^{lm}_{slr}(f,t) \simeq \frac{i\pi f L}{c} \exp\{2i\pi f k \cdot p_0/c\} n_l \cdot P_{lm} \cdot n_l. \quad (12)$$

The exponential term represents a delay-induced phase shift, commonly referred to in the literature as the Doppler phase, defined by

$$\Phi_R \equiv 2\pi f k \cdot p_0/c\,, \qquad \Delta\Phi_R = \Phi_R - \Phi_R(t = t_f^{peak}), \quad (13)$$

where $\Delta\Phi_R$ (Figure 1) is the variation of the Doppler phase with respect to its value at the signal's peak time t_f^{peak}.

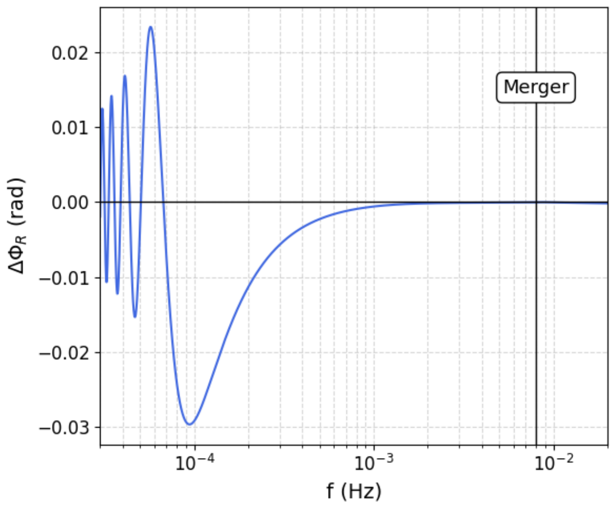

FIG. 1: Variation of the Doppler phase $\Delta\Phi_R$ as a function of frequency for a MBHB with total redshifted mass $M = 2 \times 10^6$ M$_\odot$. The vertical line indicates the merger frequency.

The Doppler phase $\Delta\Phi_R$ provides directional information about the source and encodes its angular position. At low frequencies, corresponding to the inspiral phase of the signal, which dominates the duration of the observation, the motion of the LISA constellation causes significant variation in the phase due to its displacement over time.

From Eq. (13), the Doppler phase depends on the projection $k \cdot p_0$, which measures the component of LISA's position along the direction of wave propagation. When the source lies close to LISA's orbital plane, this projection changes significantly as the constellation moves, resulting in a larger modulation of the phase. In contrast, if the source is located near the axis perpendicular to the plane, the relative position of LISA along the direction of the wave remains nearly constant, resulting in much smaller variations in the observed phase.

In Figure 1, we observe that $\Delta\Phi_R$ tends toward zero from below as the frequency increases. This behaviour indicates that $k \cdot (p_0 - p_0(t_{merger})) < 0$, meaning the gravitational wavefront reaches LISA before it would arrive at the Solar System Barycentre at the time of merger.

B. TDI transfer functions

After analysing the Doppler phase and understanding how LISA's orbital motion around the Sun modulates the gravitational wave signal, we now focus on the effect of the constellation's internal motion on the transfer function kernel $\mathcal{T}_{h_a,h_e,h_t}$ in Eq. (10), after factoring out the Doppler contribution. If this correction is not applied, the transfer functions can display artificial oscillations in frequency - especially at high frequencies - caused

As mentioned in Section III A, the low-frequency part of the signal corresponds to the inspiral phase of the binary, which lasts longer and varies slowly in amplitude. Even though the source remains in a fixed position in the sky, LISA's constellation is constantly rotating. This motion introduces time-dependent changes in the signal LISA receives, affecting both its amplitude and phase. In the frequency domain, these temporal variations appear as oscillations in the transfer functions.

However, during the merger phase of the MBHB system, the signal is extremely short in duration. During this short period, LISA's position barely shifts with respect to the source. As a result, the constellation can be treated as nearly static, and the transfer functions become smoother and more stable. This behaviour is clearly visible in channels A and E in Figure 2, where high-frequency oscillations largely disappear near the merger.

The A and E channels are constructed to cancel laser frequency noise and are designed to remain sensitive to gravitational waves over a broad frequency range. Since channels A and E are orthogonal, they can be used to reconstruct both gravitational wave polarizations.

In contrast, the T channel is optimized to suppress

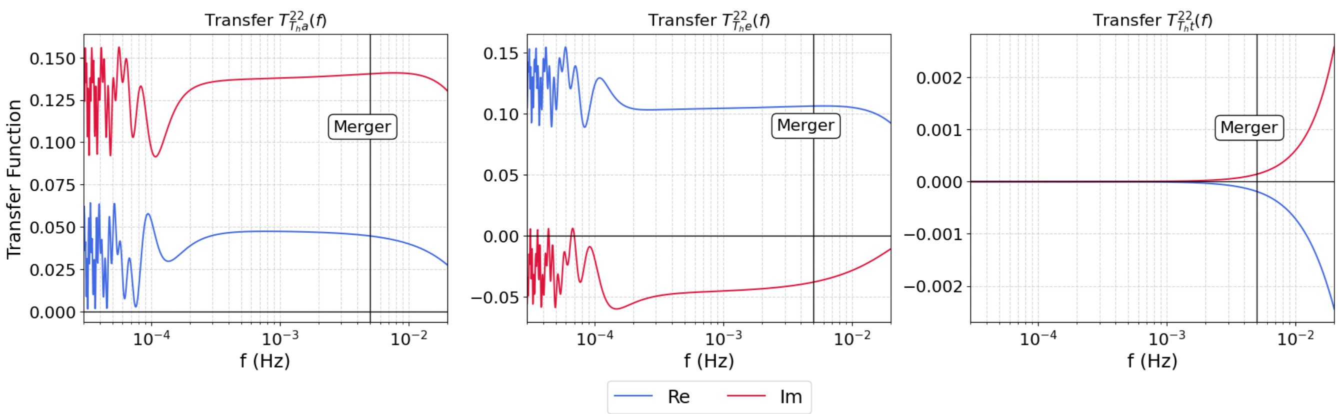

FIG. 2: Transfer functions corresponding to the TDI channels A, E, and T for the $(2,2)$ mode after factoring out the Doppler Phase and for a MBHB with total redshifted mass $M = 2\times10^6$ M$_\odot$. The blue and red curves represent the real and imaginary parts, respectively. The vertical axis is dimensionless. The vertical line marks the merger frequency of the MBHB system.

common-mode (uniform) noise across all arms of the detector. At low frequencies, where the gravitational wavelength is much larger than the constellation, all spacecraft experience nearly identical perturbations, which cancel out in T. As the frequency increases and becomes comparable to $f_L = \frac{c}{2\pi f L} \simeq 1.9\times10^{-2}$ Hz, the signal begins to affect each arm differently. This leads to a sharp increase in the channel's sensitivity, as observed in Figure 2. The T channel is especially useful for identifying residual noise and determining whether signals observed in channels A or E come from genuine gravitational waves or are just caused by the instrument, helping to avoid false detections.

C. Strain signal for LISA

Having constructed the TDI transfer functions, we can now compute the corresponding strain signals using Eq. (11). To analyse the result more effectively, we focus on the characteristic strain signal, shown in Figure 3, which is defined as

$$\tilde{h}^c_{a,e,t}(f) = 2f\tilde{h}_{a,e,t}(f). \tag{14}$$

This representation is commonly used to visualize signals in the frequency domain. It allows for direct comparison with the detector's noise curve, $\sqrt{fS_n(f)}$, where a signal above the curve suggests it could be detectable.

The overall behaviour of the strain signals in Figure 3 reflects the physical effects discussed in Section III B. For the A and E channels, we observe oscillatory patterns at low frequencies, caused by both LISA's orbital motion and internal rotation. As the frequency increases, these modulations fade and the strain becomes smoother, peaking near the merger before entering the ringdown phase and gradually decaying.

In contrast, the characteristic strain in the T channel is much lower, around six orders of magnitude below that of A and E. This is expected, as T is mainly sensitive to common-mode noise and suppresses gravitational wave signals at low frequencies. However, at higher frequencies its response grows and becomes more comparable to the other channels.

Although these results are consistent with our expectations, it is important to assess their accuracy more rigorously. Since LISA is still under development and its launch is not scheduled until around 2035, we cannot yet compare our strain signals with real data from the mission. Nevertheless, there are existing simulation frameworks and codes capable of computing LISA's response, allowing us to validate our implementation by comparing it with those results. In particular, we use the publicly available code BBHx ([6], [7], [8]) as a benchmark to test our output strain signal from Eq. (11).

A reliable method to quantify the agreement between two strain signals is through the computation of the overlap between them. For two arbitrary strains, this quantity is defined as

$$\mathcal{O}(h_1,h_2) = \frac{\langle h_1|h_2\rangle}{\sqrt{\langle h_1|h_1\rangle\cdot\langle h_2|h_2\rangle}}, \tag{15}$$

Table I presents the overlap values for each TDI channel, comparing our implementation (GWresponse) with BBHx using the IMRPhenomD model. To ensure consistency across the frequency range, we evaluate overlaps for representative low, intermediate, and high total mass binaries at redshift $z = 4$ and mass ratio $q = 2$.

The results show excellent agreement, with overlaps consistently above 0.99999999 across all TDI channels and mass ranges. Small residual differences are likely due to differences in modelling choices: our approach uses an analytical description of the spacecraft orbits, neglecting eccentricity corrections of order e^2, while BBHx relies on linear interpolation of high-precision precomputed trajectories.

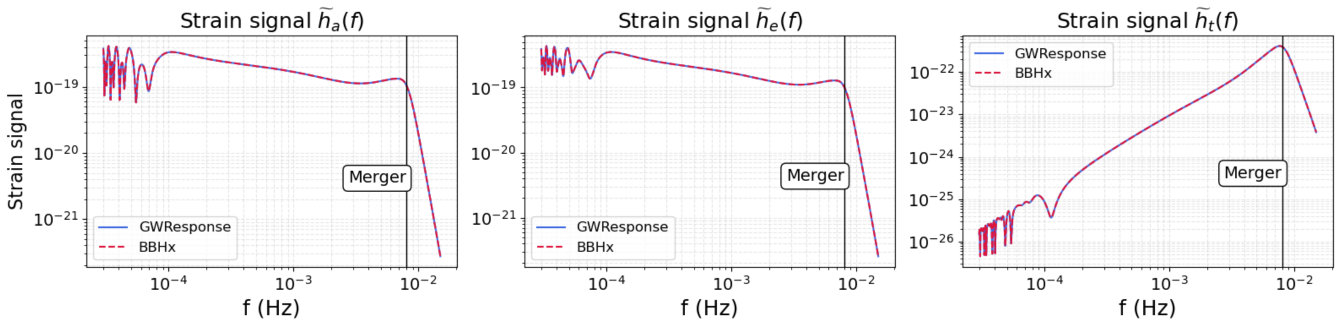

FIG. 3: Comparison of the characteristic strain signals $\tilde{h}^c_{a,e,t}(f)$ computed using our implementation (GWResponse) and the BBHx code for the TDI channels A, E, and T, based on the $(2,2)$ mode of a MBHB system with total redshifted mass $M = 2 \times 10^6\,\mathrm{M}_\odot$. The vertical line indicates the merger frequency of the system.

TABLE I: Overlap between GWresponse and BBHx strain signals in the A, E, and T channels for MBHB systems of varying total mass at redshift $z = 4$.

Total Mass ($M_\odot$)	$\mathcal{O}(A)$	$\mathcal{O}(E)$	$\mathcal{O}(T)$
1.5×10^5	0.9999999991	0.9999999993	0.9999999997
1.5×10^6	0.9999999984	0.9999999991	0.9999999995
9×10^6	0.9999999957	0.9999999982	0.9999999972

These results confirm that our frequency-domain implementation accurately reproduces the expected detector response across a wide range of source parameters, establishing a solid foundation for further analysis.

IV. CONCLUSIONS

In this work, we present the frequency-domain response of LISA using the IMRPhenomD waveform model. Throughout the process, we have verified that the behavior of the Doppler phase and the transfer functions for the A, E, and T channels are consistent with theoretical expectations. Since LISA has not yet been launched and no observational data are available, we used the BBHx code as an external reference for validating our strain signal. The resulting overlaps between our implementation and BBHx exceed 0.99999999 in all TDI channels and mass ranges, confirming the accuracy of our approach.

This foundation opens the door to further developments, such as incorporating simulations of LISA's instrumental noise via its power spectral density. This would allow for more realistic synthetic data generation, supporting future work in parameter estimation, signal recovery, and sensitivity studies. The code developed in this work is publicly available on GitHub [9].

Acknowledgments

I'm deeply grateful to Dr. Carlos Sopuerta for his constant support, guidance, and for giving me the chance to contribute—however modestly—to the LISA project. I would also like to thank Ruxandra Bondarescu for her valuable support throughout the development of this project.

[1] S. Marsat and J. G. Baker, *Fourier-domain modulations and delays of gravitational-wave signals*, (2018), arXiv:1806.10734 [gr-qc].

[2] S. Marsat, J. G. Baker, and T. Dal Canton, *Exploring the Bayesian parameter estimation of binary black holes with LISA*, (2020), arXiv:2003.00357 [gr-qc].

[3] L. J. Rubbo, N. J. Cornish, and O. Poujade, *Forward Modeling of Space-borne Gravitational Wave Detectors*, (2004), arXiv:gr-qc/0311069.

[4] S. Husa and S. Khan, *Frequency-domain gravitational waves from non-precessing black-hole binaries. I. New numerical waveforms and anatomy of the signal*, (2015), arXiv:1508.07250 [gr-qc].

[5] S. Khan and S. Husa, *Frequency-domain gravitational waves from non-precessing black-hole binaries. II. A phenomenological model for the advanced detector era*, (2015), arXiv:1508.07253 [gr-qc].

[6] M. L. Katz and S. Marsat, *GPU-accelerated massive black hole binary parameter estimation with LISA*, (2020), arXiv:2005.01827 [gr-qc].

[7] M. L. Katz, *A fully-automated end-to-end pipeline for massive black hole binary signal extraction from LISA data*, (2021), arXiv:2111.01064 [gr-qc].

[8] M. Katz, *BBHx: Fast, GPU-accelerated waveforms and response for LISA, [Software]*, 2020, https://github.com/mikekatz04/BBHx.

[9] M. Egido, *GWResponse, https://github.com/egidomireia/GWResponse.git.*

Funcions de resposta ràpida de LISA per a sistemes binaris de forats negres massius

Author: Mireia Egido Quesada, megidoqu7@alumnes.ub.edu
Facultat de Física, Universitat de Barcelona, Diagonal 645, 08028 Barcelona, Spain.

Advisor: Carlos F. Sopuerta, carlos.f.sopuerta@csic.es and
Tutor: Ruxandra Bondarescu, ruxandra.bondarescu@ub.edu

Resum: LISA és un observatori espacial d'ones gravitacionals en desenvolupament per l'Agència Espacial Europea (ESA), dissenyat per detectar senyals de baixa freqüència provinents de fonts com els sistemes binaris de forats negres massius i de massa estel·lar. Per poder processar els senyals que LISA observarà, és necessari modelitzar amb precisió la seva resposta instrumental. En aquest treball, implementem la resposta de LISA en el domini de freqüències sense soroll utilitzant el model d'ona IMRPhenomD. La implementació s'ha realitzat amb JAX, que permet un càlcul numèric eficient i suporta la diferenciació automàtica. El nostre model té en compte el moviment de la constel·lació i els observables de la Interferometria amb Retard Temporal (TDI). Els senyals resultants es validen amb el codi de simulació BBHx, obtenint solapaments superiors a 0.99999999 en tots els canals TDI, fet que confirma la precisió del nostre enfocament.
Paraules clau: Ones gravitacionals, Interferometria, Modelització numèrica, Anàlisi de Fourier

ODSs: Aquest treball esta relacionat amb l'Objectiu de Desenvolupament Sostenible (ODS) 9

Objectius de Desenvolupament Sostenible (ODSs o SDGs)

1. Fi de la es desigualtats		10. Reducció de les desigualtats	
2. Fam zero		11. Ciutats i comunitats sostenibles	
3. Salut i benestar		12. Consum i producció responsables	
4. Educació de qualitat		13. Acció climàtica	
5. Igualtat de gènere		14. Vida submarina	
6. Aigua neta i sanejament		15. Vida terrestre	
7. Energia neta i sostenible		16. Pau, justícia i institucions sòlides	
8. Treball digne i creixement econòmic		17. Aliança pels objectius	
9. Indústria, innovació, infraestructures	X		

Aquest treball s'alinea amb l'Objectiu de Desenvolupament Sostenible (ODS) número 9: Indústria, innovació i infraestructura, concretament amb la fita 9.5, en tant que contribueix a la investigació científica i al desenvolupament de mètodes computacionals eficients per a l'anàlisi de dades en missions espacials com LISA. Aquests avenços formen part del progrés tecnològic necessari per al desenvolupament d'infraestructures científiques de nova generació.

Appendix A: Fourier transform of the signal

As outlined in Section I, the objective of this work is to compute the detector response in the frequency domain in a computationally efficient way. Following Eq. (2), the detected signal $s(t)$ can be expressed as

$$s(t) = F(t)h(t + d(t)). \tag{A1}$$

where $h(t)$ is the gravitational wave signal, $d(t)$ represents the time-dependent delay, and $F(t)$ is a time-varying prefactor that encapsulates the relevant geometric projection effects. In other words, each individual contribution to the detector output can be described as a delayed version of the full waveform, modulated by a geometric factor.

A common approach is to express the signal in terms of a frequency-domain transfer function:

$$\widetilde{s}(f) = \mathcal{T}(f)\widetilde{h}(f), \tag{A2}$$

where $\mathcal{T}(f)$ is the transfer function that translates the frequency-domain gravitational wave signal $\widetilde{h}(t)$ into the detector response $\widetilde{s}$(f). To construct this function, we begin by rewriting the time-delayed waveform in the frequency domain as

$$h_d(t) = h(t + d(t)) = \int_{-\infty}^{\infty} df e^{-2i\pi f(t+d(t))}\widetilde{h}(f), \tag{A3}$$

and the signal in the frequency domain becomes

$$\begin{aligned}\widetilde{s}(f) &= (\widetilde{F \times h_d})(f)\\ &= \int_{-\infty}^{\infty} dt e^{2i\pi f t} F(t) \int_{-\infty}^{\infty} df' e^{-2i\pi f'(t+d(t))}\widetilde{h}(f')\\ &= \int_{-\infty}^{\infty} df'\widetilde{h}(f-f') \int_{-\infty}^{\infty} dt e^{2i\pi f' t} e^{-2i\pi f'(t+d(t))} F(t).\end{aligned} \tag{A4}$$

In the last step, we have performed the variable change $f' \to f - f'$. This expression can also be written as a generalized convolution integral with a frequency-dependent kernel:

$$\widetilde{s}(f) = \int_{-\infty}^{\infty} df'\widetilde{h}(f-f')\widetilde{G}(f-f', f'). \tag{A5}$$

with $\widetilde{G}(f - f', f')$ encoding the effects of time-varying delays and geometric modulation. We can now define the frequency-dependent kernel $\widetilde{G}(f, f')$, along with its time-domain counterpart $G(f, t)$, as follows:

$$G(f, t) = e^{-2i\pi f d(t)} F(t), \tag{A6a}$$

$$\widetilde{G}(f, f') = \int_{-\infty}^{\infty} dt e^{2i\pi f' t} G(f, t). \tag{A6b}$$

Replacing Eq.(A6) into Eq.(A5) can be computationally expensive. However, efficient approximations can be made to reduce the overall cost. In particular, for slowly varying modulations and delays, the Fourier transform $\widetilde{G}(f, f')$ is expected to be localized in the interval $f' \in [-f_{\max}, f_{\max}]$, where $f_{\max}$ is roughly the inverse of the characteristic timescale of the modulation.

Under this approximation, the waveform only needs to be evaluated near the frequency f. This allows us to perform a formal leading-order expansion of $\widetilde{h}(f - f')$ around f, treating the amplitude as constant and expanding the phase to first order:

$$\widetilde{h}(f - f') \simeq A(f) \exp\left\{-i\left(\Psi(f) - f'\frac{d\Psi}{df}\right)\right\}. \tag{A7}$$

Applying this approximation to Eq. (A5), we obtain:

$$\widetilde{s}(f) = \widetilde{h}(f)\int_{-\infty}^{\infty} df e^{if'\frac{d\Psi}{df}}\widetilde{G}(f) = \widetilde{h}(f)G\left(f, -\frac{1}{2\pi}\frac{d\Psi}{df}\right), \tag{A8}$$

so the response is approximately reduced to evaluating the modulation and delay at a representative, signal-dependent time t_f, defined as

$$t_f = -\frac{1}{2\pi}\frac{d\Psi}{df}. \tag{A9}$$

By comparing Eq.(A8) with Eq.(A2), we identify the transfer function as

$$\mathcal{T}(f) = G(f, t_f) = F(t_f)e^{-2i\pi f d(t_f)}. \tag{A10}$$

This expression shows that the frequency-domain signal $\widetilde{s}(f)$ is obtained by multiplying the waveform $\widetilde{h}(f)$ by a response factor evaluated at the representative time t_f. The delay contributes a linear phase term, with $d(t_f)$ effectively treated as a constant time shift.

From Eq.(2) and Eq.(A1), we define the time-dependent prefactor as

$$F_{slr}(t) = \frac{1}{2}\frac{1}{1 - k\cdot n_l(t)} n_l(t)\cdot P_{lm}\cdot n_l(t). \tag{A11}$$

Taking into account the orbital delays $-k\cdot p_{s,r}(t)$ for the sending and receiving spacecraft, respectively, we obtain

$$G_{slr} = F_{slr}(t)\left(e^{-2i\pi f(-k\cdot p_s(t))-L)} - E^{-2i\pi f(-k\cdot p_r(t))}\right). \tag{A12}$$

This expression can be rewritten as

$$\begin{aligned}G_{slr} = \frac{i\pi f L}{c} &sinc[\pi f L/c(1 - k\cdot n_l)]\\ &\cdot \exp\{i\pi f[L + k\cdot(p_r + p_s)]/c\} n_l\cdot P_{lm}\cdot n_l,\end{aligned} \tag{A13}$$

where, in this work, we consider $l = 2$ and $m = \pm 2$. The transfer function is then obtained by evaluating Eq.(7) at the representative time t_f defined in Eq.(8):

$$\mathcal{T}_{slr}(f) = G_{slr}(f, t_f). \tag{A14}$$

Appendix B: Time Delay Interferometry

Although the one-arm observables defined in Eq. (2) represent the raw signals measured by LISA, their amplitude is many orders of magnitude smaller than the laser frequency noise. As a result, the gravitational wave signal would be entirely buried in noise without further processing. To address this, we apply Time Delay Interferometry (TDI), a technique that constructs new observables from specific combinations of the y_{slr} terms to effectively cancel out the dominant laser noise.

In this work, we consider first-generation TDI, which is compatible with our assumption of a rigid and non-rotating constellation. More advanced generations of TDI take into account the time-dependent armlengths and rotational motion of LISA.

The first-generation Michelson TDI observable X is defined as

$$\begin{aligned} X = y_{31} + y_{13,L} + (y_{21} + y_{12,L})_{,2L} \\ - (y_{21} + y_{12,L}) - (y_{31} + y_{13,L})_{,2L}, \end{aligned} \tag{B1}$$

where time delays are indicated by subscripts, i.e, $y_{slr,nL}$ represents $y_{slr}(t - nL/c)$. The other Michelson observables Y and Z are obtained through cyclic permutation of the indices.

From the observables X, Y, and Z, we can construct a new set of independent and uncorrelated channels A, E, and T assuming equal and uncorrelated noise across the arms. These are defined as:

$$A = \frac{1}{\sqrt{2}}(Z - X), \tag{B2a}$$

$$E = \frac{1}{\sqrt{6}}(X - 2Y + Z), \tag{B2b}$$

$$T = \frac{1}{\sqrt{3}}(X + Y + Z). \tag{B2c}$$

In terms of the channel definitions in Eq. B2, the TDI observables can be expressed in the frequency domain through the following rescalings:

$$\tilde{a}\,,\tilde{e} = \frac{e^{-2i\pi fL/c}}{i\sqrt{2}sin(2\pi fL/c)} \times \tilde{A}, \tilde{E}, \tag{B3a}$$

$$\tilde{t} = \frac{e^{-3i\pi fL/c}}{2\sqrt{2}sin(\pi fL/c)sin(2\pi fL/c)} \times \tilde{T}. \tag{B3b}$$

Defining $z \equiv \exp(2i\pi fL/c)$, the TDI channels can be rewritten in terms of the y_{slr} observables as

$$\tilde{a} = (1 + z)(\tilde{y}_{31} + \tilde{y}_{13}) - \tilde{y}_{23} - z\tilde{y}_{32} - \tilde{y}_{21} - z\tilde{y}_{12}, \tag{B4a}$$

$$\begin{aligned} \tilde{e} = \frac{1}{\sqrt{3}}[(1 - z)(\tilde{y}_{13} - \tilde{y}_{31}) + (2 + z)(\tilde{y}_{12} - \tilde{y}_{32}) \\ + (1 + 2z)(\tilde{y}_{21} - \tilde{y}_{23})], \end{aligned} \tag{B4b}$$

$$\tilde{t} = \sqrt{\frac{2}{3}}[\tilde{y}_{21} - \tilde{y}_{12} + \tilde{y}_{32} - \tilde{y}_{23} + \tilde{y}_{13} - \tilde{y}_{31}]. \tag{B4c}$$

We can model these reduced channels using transfer functions of the form

$$\tilde{a}, \tilde{e}, \tilde{t} = \mathcal{T}_{a,e,t}(f)\tilde{h}(f). \tag{B5}$$

Finally, to relate these combinations directly to the gravitational strain, we introduce the following rescaled definitions

$$\tilde{h}_{a,e,t} \equiv \frac{1}{(-6i\pi fL/c)} \times \tilde{a}, \tilde{e}, \tilde{t}, \tag{B6a}$$

$$\mathcal{T}_{h_a,h_e,h_t} \equiv \frac{1}{(-6i\pi fL/c)}\mathcal{T}_{a,e,t}. \tag{B6b}$$